JCTC Journal of Chemical Theory and Computation

pubs.acs.org/JCTC Article

Combining Renormalized Singles *GW* Methods with the Bethe–Salpeter Equation for Accurate Neutral Excitation Energies

Jiachen Li, Dorothea Golze, and Weitao Yang*

Cite This: *J. Chem. Theory Comput.* 2022, 18, 6637–6645 Read Online

ACCESS | Metrics & More | Article Recommendations | Supporting Information

ABSTRACT: We apply the renormalized singles (RS) Green's function in the Bethe–Salpeter equation (BSE)/*GW* approach to predict accurate neutral excitation energies of molecular systems. The BSE calculations are performed on top of the $G_{RS}W_{RS}$ method, which uses the RS Green's function also for the computation of the screened Coulomb interaction *W*. We show that the BSE/$G_{RS}W_{RS}$ approach significantly outperforms BSE/G_0W_0 for predicting excitation energies of valence, Rydberg, and charge-transfer (CT) excitations by benchmarking the Truhlar–Gagliardi set, Stein CT set, and an atomic Rydberg test set. For the Truhlar–Gagliardi test set, BSE/$G_{RS}W_{RS}$ provides comparable accuracy to time-dependent density functional theory (TDDFT) and is slightly better than BSE starting from eigenvalue self-consistent *GW* (ev*GW*). For the Stein CT test set, BSE/$G_{RS}W_{RS}$ significantly outperforms BSE/G_0W_0 and TDDFT with the accuracy comparable to BSE/ev*GW*. We also show that BSE/$G_{RS}W_{RS}$ predicts Rydberg excitation energies of atomic systems well. Besides the excellent accuracy, BSE/$G_{RS}W_{RS}$ largely eliminates the dependence on the choice of the density functional approximation. This work demonstrates that the BSE/$G_{RS}W_{RS}$ approach is accurate and efficient for predicting excitation energies for a broad range of systems, which expands the applicability of the BSE/*GW* approach.

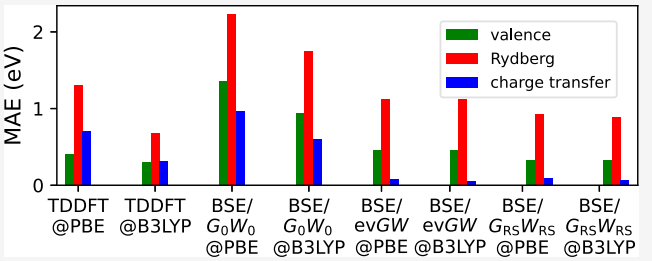

1. INTRODUCTION

The accurate prediction of neutral excitation energies from first-principle calculations plays a critical role in guiding the understanding and new developments in chemistry, biochemistry, and material science, such as drug delivery[1,2] and design of an organic sensitizer.[3,4] In the past decades, many theoretical approaches have been developed to compute accurate excitation energies. Time-dependent density functional theory[5−7] (TDDFT) ranks among the most popular approaches. Because of the good accuracy and the affordable computational cost, TDDFT has been widely implemented in modern quantum chemistry packages to calculate energies, structures, and other properties of excited states for molecular and periodic systems.[8−10] However, TDDFT has several well-known shortcomings. For example, TDDFT with commonly used density functional approximations (DFAs) poorly predicts excitation energies of Rydberg and charge-transfer (CT) excitations.[11,12] The failure of TDDFT for these excitations must be attributed to the incorrect description of the long-range behavior using conventional DFAs.[11,12] Attempts to address this issue include the usage of range-separated or Coulomb-attenuated functionals[13−16] and tuning the fraction of the Hartree–Fock (HF)[17,18] exchange in DFAs.[19] In addition, the accuracy of TDDFT strongly depends on the exchange–correlation (XC) kernel, which is the second derivative of the XC energy from the given DFA with respect to the electron density.[10,20] The difference in the calculated excitation energies obtained from TDDFT with different DFAs can exceed 1.0 eV for valence excitations and even exceed 2.0 eV for Rydberg excitations.[10,21] Recent developments to improve the accuracy of TDDFT include multireference DFT,[22,23] orbital-optimized DFT,[24] and mixed-reference spin-flip TDDFT.[25]

In the last years, the Bethe–Salpeter equation[26−28] (BSE) formalism in the Green's function many-body perturbation theory[29,30] has become increasingly popular for computing the optical excitations of molecules[31] and has been most recently also applied to K-edge transitions.[32] BSE is commonly performed on top of a *GW* calculation[30,33,34] using the *GW* quasiparticle (QP) energies as the input. We denote this approach as BSE/*GW*. Recently, BSE in combination with the T-matrix approximation for predicting neutral excitation energies has also been reported.[35] In the BSE/*GW* approach, the electron–hole interaction is described by the screened Coulomb interaction *W* instead of the bare Coulomb interaction. The *GW* QP energies substantially improve upon the Kohn–Sham (KS) orbital energies for predicting fundamental HOMO–LUMO gaps and ionization potentials

Received: June 30, 2022
Published: October 24, 2022

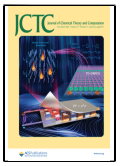

in general, which are the critical quantities in BSE to calculate excitation energies. BSE/*GW* has been successfully applied to calculate excitation energies for systems of different sizes including molecules, solids, and low-dimensional materials.[32,36−49]

However, the BSE/*GW* approach still suffers from several problems. First, although BSE has a computationally favorable scaling of $O(N^4)$ with respect to the system size N, which is the same as in TDDFT, the preceding *GW* calculation is computationally demanding. In the fully analytical treatment of the *GW* self-energy, the diagonalization of the random phase approximation (RPA) equation scales as $O(N^6)$ and the self-energy evaluation scales as $O(N^5)$.[34,50] Thus, the computationally expensive *GW* step dominates the computational cost in a BSE/*GW* calculation. Many techniques have been developed to reduce the computational cost of *GW* calculations, for example, the contour deformation technique[51] or analytic continuation of the self-energy,[52,53] which scales $O(N^4)$ for valence states. The computational cost is further reduced in cubic scaling *GW* implementations, which recently emerged for localized basis set codes[54−57] enabling *GW* calculations for large systems of more than thousand atoms.

Second, the accuracy of the commonly used BSE/G_0W_0 approach has an undesirable dependence on the choice of the DFA,[58,59] which is due the perturbative nature of the G_0W_0 scheme. In BSE/G_0W_0, the dependence on the DFA starting point is in the range of 0.5 eV for predicting valence excitation energies and can even exceed 1.0 eV for predicting CT excitation energies.[59] It has been shown that BSE/G_0W_0 based on range-separated functionals and tuned hybrid functionals provides more accurate excitation energies[32,60] than BSE/G_0W_0 based on GGA functionals. This dependence can be largely reduced by introducing self-consistency into the *GW* calculations, such as the eigenvalue-self-consistent *GW* (ev*GW*) method, where the eigenvalues are iterated in G and W, the quasiparticle-self-consistent *GW* (qs*GW*) scheme,c[61,62] or the fully self-consistent *GW* (sc*GW*) approach.[63,64] It has been shown that the BSE/ev*GW* approach provides an accuracy comparable to TDDFT for predicting valence excitations and significantly outperforms BSE/G_0W_0 and TDDFT for predicting CT and Rydberg excitations.[38,59,65] The DFA dependence in BSE/ev*GW* is largely washed out.[38,59,65] In practice, ev*GW* calculations can converge within a few steps by using the linear mixing method.[62] However, ev*GW* might have convergence difficulties for systems with multiple solutions.[66,67] In addition, the extra computational cost in ev*GW* is expensive for large systems.

To reduce the computational cost, efforts were recently made to approximate the *GW* QP energies by improved orbital energies from DFT and to use the latter as the BSE input. For example, we recently employed the localized orbital scaling correction[68] (LOSC), which minimizes the delocalization error in DFAs to predict orbital energies. We showed that the BSE/LOSC approach provides good accuracy for predicting excitation energies of different systems[59] and yields significantly better results than BSE/G_0W_0. The BSE/LOSC approach scales as $O(N^4)$ complexity. Another computationally cheaper BSE approach is based on Koopmans-compliant (KC) functionals, where the orbital energies are derived from KC functionals and the screened interaction is obtained via direct minimization on top of a maximally localized Wannier function basis.[69] The KC-based BSE yields similar accuracy as the BSE/G_0W_0 method.[69]

In this work, we applied the recently developed renormalized singles (RS) Green's function[70,71] in BSE/*GW* to compute accurate excitation energies with affordable computational cost. The idea of the RS Green's function approach is to compute the HF self-energy with the KS orbitals from DFT[72−74] instead of the HF orbitals. Because of Brillouin's theorem,[18] there is no singles contribution to the HF self-energy in the perturbation. However, the HF Green's function is not a good starting point for G_0W_0 calculations.[70,75] Therefore, the HF Hamiltonian is constructed with KS orbitals and diagonalized separately in the occupied and virtual subspaces. This renormalization procedure absorbs all singles contributions into the self-energy to reduce the dependence on the choice of the DFA. The resulting RS Green's function is constructed with RS orbital energies from the renormalization process, which has the same form as the KS Green's function. From the viewpoint of the RPA, higher order contributions are also included in the infinite summation by this renormalization process. Compared with the self-consistent *GW* methods that solve Hedin's equations iteratively to eliminate the starting point dependence, the one-shot RS process captures all contributions of the single excitations while hardly increasing the computational compared to G_0W_0. The RS Green's function has been used in the *GW* methods and T-matrix methods to predict accurate QP energies for valence and core states.[59,70,76] The concept of RS has also been used in the multireference DFT approach[23] to describe the static correlation in strongly correlated systems. The RS Green's function shares similar thinking as the RS excitation in the RPA calculation for correlation energies.[77−79]

The RS Green's function has been applied in the *GW* approximation in two flavors. The first one is the $G_{RS}W_0$[70] method, which uses the RS Green's function as a new starting point and calculates the screened interaction with the KS Green's function. We found that the $G_{RS}W_0$ method provides a considerable improvement over G_0W_0 for predicting valence ionization potentials and electron affinities with a reduced starting point dependence[70] but fails to restore the correct physics for deep core excitations.[71] The second one is the $G_{RS}W_{RS}$ method,[71] which uses the RS Green's function as a new starting point and calculates the screened interaction with the RS Green's function. We found that $G_{RS}W_{RS}$ also yields an improvement over G_0W_0,[80] that is, it opens the fundamental gaps compared to G_0W_0 similar to ev*GW*; see also Section 1 in the Supporting Information. Because of the nonlinear nature of the QP equation, multiple solutions can be found due to the unphysical discontinuities and intruder states,[66,67,81] especially for core states. $G_{RS}W_{RS}$ properly separates the main core QP state from the satellites and provides a solution to the QP equation corresponding to the desired core state,[71] which is not the case for G_0W_0 with GGA or hybrid functionals with a low amount of exact exchange. Even though the absolute core-level energies are overestimated by several electronvolts, the relative shifts are predicted with a reasonable accuracy.[71] For valence as well as core states, the starting point dependence is significantly reduced compared to G_0W_0.

In the present work, we benchmark both RS flavors, BSE/$G_{RS}W_0$ and BSE/$G_{RS}W_{RS}$, for the prediction of neutral excitations of molecular systems, including valence, CT, and Rydberg excitations.

https://doi.org/10.1021/acs.jctc.2c00686
J. Chem. Theory Comput. 2022, 18, 6637−6645

2. THEORY

2.1. RS Green's Function. The goal of the RS Green's function approach is to improve the accuracy of perturbative *GW* methods by including exactly the exchange self-energy, which is a one-electron contribution, and reduce the starting point dependence of the orbital energies on the DFA. The general idea is to construct the HF self-energy from KS orbitals, followed by a separate diagonalization in the occupied orbital subspace and the virtual orbital subspace.[70] Effectively, the RS approach treats the one-body exchange self-energy exactly, or nonperturbatively, by diagonalization, unlike the commonly used G_0W_0 approach, in which the one-body exchange is included perturbatively along with the many-body correlation self-energy. The RS Green's function G_{RS} is defined as the solution of the two projected equations in the occupied orbital subspace and the virtual orbital subspace[70]

$$P(G_{RS}^{-1})P = P(G_0^{-1})P + P(\Sigma_{Hx}[G_0] - v_{Hxc})P \tag{1}$$

and

$$Q(G_{RS}^{-1})Q = Q(G_0^{-1})Q + Q(\Sigma_{Hx}[G_0] - v_{Hxc})Q \tag{2}$$

where $P = \sum_i^{occ} |\psi_i\rangle\langle\psi_i|$ is the projection into the occupied orbital space and $Q = I - P$ is the projection into the virtual orbital space, ψ is the KS orbital, Σ_{Hx} is the Hartree-exchange self-energy, and v_{Hxc} is the Hartree-exchange−correlation potential. $\Sigma_{Hx}[G_0]$ means that the HF self-energy (Hartree and exchange contribution) is constructed from the KS density matrix. Equivalently, the RS Green's function is obtained by using the DFA density matrix in the HF Hamiltonian, namely, $H_{HF}[G_0]$, and solving two projected HF equations in the occupied and virtual subspaces[70]

$$P(H_{HF}[G_0])P|\psi_i^{RS}\rangle = \epsilon_i^{RS}P|\psi_i^{RS}\rangle \tag{3}$$

and

$$Q(H_{HF}[G_0])Q|\psi_a^{RS}\rangle = \epsilon_a^{RS}Q|\psi_a^{RS}\rangle \tag{4}$$

where ϵ^{RS} is the RS orbital energy and ψ^{RS} is the RS orbital. Here, we use *i*, *j*, *k*, *l* for occupied orbitals, *a*, *b*, *c*, *d* for virtual orbitals, *p*, *q*, *r*, *s* for general orbitals. The subspace diagonalization of the HF Hamiltonian is performed only once. The resulting RS Green's function is diagonal in the occupied and virtual subspaces[70]

$$[G_{RS}(\omega)]_{pq} = \delta_{pq}\frac{1}{\omega - \epsilon_p^{RS} + i\eta\mathrm{sgn}(\epsilon_p^{RS} - \mu)} \tag{5}$$

Here, μ is the chemical potential and η is the broadening parameter. As shown in eq 5, the RS Green's function has a similar form as the KS Green's function except that the KS orbital energies in the denominator are replaced by the RS orbital energies. Therefore, the RS Green's function can be directly implemented in existing *GW* codes.

2.2. $G_{RS}W_0$ and $G_{RS}W_{RS}$. The RS Green's function is used in two *GW* flavors: $G_{RS}W_0$[70] and $G_{RS}W_{RS}$.[71] In both methods, KS orbitals instead of RS orbitals are used for simplicity[70,71] because using the RS orbitals does not change the results significantly. Therefore, the exchange part of the self-energy in $G_{RS}W_0$ and $G_{RS}W_{RS}$ is the same as G_0W_0. In $G_{RS}W_0$,[70] the RS Green's function is used as the starting point and the screened interaction is calculated with the KS Green's function, which means the KS Green's function is used in the RPA calculation. The correlation part of the self-energy in $G_{RS}W_0$ is[70]

$$[\Sigma_c^{G_{RS}W_0}(\omega)]_{pp} = \sum_m \sum_q \frac{|(pq|\rho_m^{KS})|^2}{\omega - \epsilon_q^{RS} - (\Omega_m^{KS} - i\tilde{\eta})\mathrm{sgn}(\epsilon_q^{RS} - \mu)} \tag{6}$$

where ρ_m^{KS} and Ω_m^{KS} are the transition density and the excitation energy from RPA calculated with the KS Green's function, *m* is the index for the RPA excitation, and $\tilde{\eta} = 3\eta$.[50]

With the self-energy in eq 6, the QP equation for $G_{RS}W_0$ is[70]

$$\epsilon_p^{QP} = \epsilon_p^0 + \langle p|\Sigma_{xc}^{G_{RS}W_0}(\epsilon_p^{QP}) - v_{xc}|p\rangle \tag{7}$$

where ϵ_p^0 is the KS orbital energy. In eq 7, the QP energy ϵ_p^{QP} appears in both sides, which means eq 7 needs to be solved iteratively. To reduce the computational cost, eq 7 can be linearized[30,70] as

$$\epsilon_p^{QP} = \epsilon_p^0 + Z_p^{G_{RS}W_0}\langle p|\Sigma_{xc}^{G_{RS}W_0}(\epsilon_p^{RS}) - v_{xc}|p\rangle \tag{8}$$

with the factor $Z_p^{G_{RS}W_0} = \left(1 - \frac{\partial[\Sigma_c^{G_{RS}W_0}(\omega)]_{pp}}{\partial\omega}|_{\omega=\epsilon_p^{RS}}\right)^{-1}$.

The $G_{RS}W_{RS}$ method[71] uses the RS Green's function as a new starting point and calculates the screened interaction with the RS Green's function, which means that the RS Green's function is used in the RPA calculation. The correlation part of the self-energy in $G_{RS}W_{RS}$[71]

$$[\Sigma_c^{G_{RS}W_{RS}}(\omega)]_{pp} = \sum_m \sum_q \frac{|(pq|\rho_m^{RS})|^2}{\omega - \epsilon_q^{RS} - (\Omega_m^{RS} - i\tilde{\eta})\mathrm{sgn}(\epsilon_q^{RS} - \mu)} \tag{9}$$

where ρ_m^{RS} and Ω_m^{RS} are the transition density and the excitation energy from RPA calculated with the RS Green's function.

Therefore, the QP equation for $G_{RS}W_{RS}$ is[71]

$$\epsilon_p^{QP} = \epsilon_p^0 + \langle p|\Sigma_{xc}^{G_{RS}W_{RS}}(\epsilon_p^{QP}) - v_{xc}|p\rangle \tag{10}$$

Equation 10 can also be linearized as

$$\epsilon_p^{QP} = \epsilon_p^0 + Z_p^{G_{RS}W_{RS}}\langle p|\Sigma_{xc}^{G_{RS}W_{RS}}(\epsilon_p^{RS}) - v_{xc}|p\rangle \tag{11}$$

with the factor $Z_p^{G_{RS}W_{RS}} = \left(1 - \frac{\partial[\Sigma_c^{G_{RS}W_{RS}}(\omega)]_{pp}}{\partial\omega}|_{\omega=\epsilon_p^{RS}}\right)^{-1}$.

As shown in ref 34, the linearized QP equation gives small errors for valence QP energy calculations, which are important in BSE. In Section 2 in the Supporting Information, we show that using linearized QP equations defined in eqs 8 and 11 gives small differences around 0.01 eV compared to eqs 7 and 10 for the type of excitations studied here. Therefore, the linearized QP equations are solved to reduce the computational cost in the present work.

2.3. BSE/$G_{RS}W_0$ and BSE/$G_{RS}W_{RS}$ Approaches. The QP energies obtained from $G_{RS}W_{RS}$ are used in BSE to calculate the excitation energies. With the static approximation for the screened interaction that treats the frequency as zero,[31,82,83] the working equation of BSE is a generalized eigenvalue equation,[31,82,83] which is similar to the Casida equation in TDDFT[6,7]

$$\begin{bmatrix} \mathbf{A} & \mathbf{B} \\ \mathbf{B}^* & \mathbf{A}^* \end{bmatrix}\begin{bmatrix} \mathbf{X} \\ \mathbf{Y} \end{bmatrix} = \Omega\begin{bmatrix} \mathbf{I} & \mathbf{0} \\ \mathbf{0} & -\mathbf{I} \end{bmatrix}\begin{bmatrix} \mathbf{X} \\ \mathbf{Y} \end{bmatrix} \tag{12}$$

where Ω is the excitation energy. In eq 12 the **A**, **B** matrices are defined as

https://doi.org/10.1021/acs.jctc.2c00686
J. Chem. Theory Comput. 2022, 18, 6637−6645

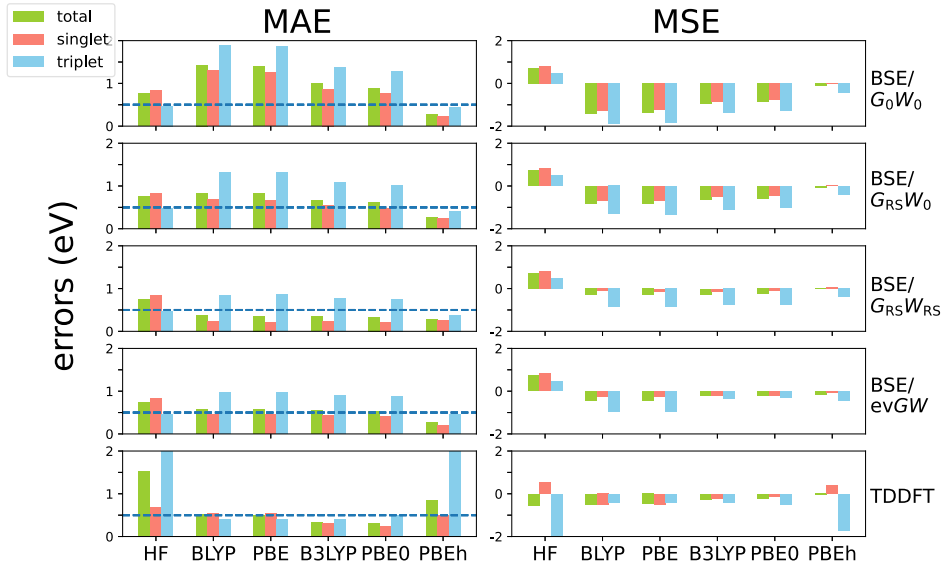

Figure 1. MAEs and MSEs of excitation energies in the Truhlar−Gagliardi test set obtained from TDDFT, BSE/G_0W_0, BSE/$G_{RS}W_0$, BSE/$G_{RS}W_{RS}$, and BSE/evGW based on HF, BLYP, PBE, B3LYP, PBE0, and PBEh(0.75). Reference values for pNA and DMABN were taken from ref 94 and for the remaining molecules from ref 95. The reference values are the theoretical best estimates. The aug-cc-pVDZ basis set was used for naphthalene, pNA, and DMABN, and the aug-cc-pVTZ basis set was used for the remaining systems. B-TCNE was excluded due to the high computational cost. Total MAEs and total MSEs were calculated by averaging all systems with equal weights. The error for system i is defined as $\text{Error}_i = E_i^{\text{calc}} - E_i^{\text{reference}}$.

$$A_{ia,jb} = \delta_{ij}\delta_{ab}(\epsilon_a^{\text{QP}} - \epsilon_i^{\text{QP}}) + v_{ia,jb} - W_{ij,ab}(\omega = 0) \tag{13}$$

$$B_{ia,jb} = v_{ia,bj} - W_{ib,aj}(\omega = 0) \tag{14}$$

where v is the Coulomb interaction and $W(\omega = 0)$ is the static screened interaction. v is the Coulomb interaction defined as

$$v_{pq,rs} = \int \mathrm{d}x_1 \mathrm{d}x_2 \frac{\psi_p^*(x_1)\psi_r^*(x_2)\psi_q(x_1)\psi_s(x_2)}{|\mathbf{r}_1 - \mathbf{r}_2|} \tag{15}$$

where $\{\psi_p\}$ is the set of input orbitals and x is the combined space-spin variable for (r, σ). W is the screened interaction defined as

$$W_{pq,rs} = \sum_{tu} (D^{-1})_{pq,tu} v_{tu,rs} \tag{16}$$

where the dielectric function D is calculated by the static response function χ[82,83]

$$D_{pq,rs} = \delta_{pr}\delta_{qs} - v_{pq,rs}\chi_{rs,rs} \tag{17}$$

$$\chi_{ia,ia} = \chi_{ai,ai} = (\epsilon_i^{\text{QP}} - \epsilon_a^{\text{QP}})^{-1} \tag{18}$$

The BSE working equation in eq 12 is analogous to the Casida equation[6,7] in TDDFT. The only difference is that the BSE kernel replaces the XC kernel. Thus, the scaling of solving eq 12 is $O(N^4)$ by using the canonical Davidson algorithm.[84,85]

3. COMPUTATIONAL DETAILS

We implemented the BSE/$G_{RS}W_0$ and BSE/$G_{RS}W_{RS}$ approaches in the QM4D quantum chemistry package[86] and applied them to calculate the excitation energies of different systems. As discussed in ref 59, the application of the Tamm−Dancoff approximation (TDA) improves the accuracy of BSE/G_0W_0 for predicting both singlet and triplet excitation energies because BSE/G_0W_0 largely underestimates the excitation energies of molecular systems. However, for BSE/$G_{RS}W_{RS}$ and BSE/evGW, which predict larger excitation energies than BSE/G_0W_0, using TDA leads to similar or worse triplet results and worsens singlet results as shown in Section 4 in the Supporting Information and ref 38. In addition, as shown in recent studies, using TDA in BSE/GW can lead to blueshifts in nanosized systems[87−89] and worse accuracy for singlet-triplet energy gaps in organic molecules.[36] Therefore, TDA is not used in the present work. We tested three different sets: the comprehensive Truhlar−Gagliardi test set[90] that contains singlet, triplet, valence, CT, and Rydberg excitations, the Stein CT test set[91] that contains 12 intramolecular CT excitations between an aromatic donor and the tetracyanoethylene acceptor, and a test set for Rydberg excitations that contains three atomic systems. For the Truhlar−Gagliardi test set,[90] the aug-cc-pVTZ basis set[92,93] was used for all molecules, except for naphthalene, pNA, and DMABN, for which the aug-cc-pVDZ basis set[92,93] was employed. It has been shown that the aug-cc-pVTZ basis sets yield converged neutral optical excitations,[46] and even aug-cc-pVDZ results were found to deviate by not more than 0.2−0.3 eV from the basis set limit.[46] B-TCNE was excluded due to the high computational cost. Reference values for pNA and DMABN were taken from refs 94 and 95 for the remaining molecules in the Truhlar−Gagliardi test set. The reference values are the theoretical best estimates, for example, using FCI or CCSDTQ.[94,95] Geometries were all taken from ref 90. Note that geometries used in ref 95 are slightly different from those in the Truhlar−Gagliardi set. As shown in refs 95 and 96, the difference between theoretical best estimates obtained with two slightly different geometries is around 0.01 eV. Thus, we do not expect the small differences to change the conclusion. For the Stein CT test set,[91] the cc-pVDZ[92] basis set was used. Because theory best estimates for the Stein CT test set are not available, the experimental values in the gas phase[91] were taken as the reference, which can be a source of errors. For the test of Rydberg excitation energies of B^+, Be, and Mg, the aug-cc-

https://doi.org/10.1021/acs.jctc.2c00686
J. Chem. Theory Comput. 2022, 18, 6637−6645

pVQZ basis set[92,93] was employed. Experimental reference values were taken from ref 97. TDDFT calculations were performed with the GAUSSIAN16 A.03 software.[98] BSE/G_0W_0, BSE/$G_{RS}W_0$, BSE/$G_{RS}W_{RS}$, and evGW calculations were performed with QM4D. QM4D uses Cartesian basis sets and uses the resolution of identity technique[52,99,100] to compute two-electron integrals. All basis sets and corresponding fitting basis sets were taken from the basis set exchange.[101−103]

4. RESULTS

4.1. Truhlar−Gagliardi Test Set. We first examine the performance of the BSE/$G_{RS}W_{RS}$ approach for predicting the excitation energies of molecules from the Truhlar−Gagliardi test set. Excluding B-TCNE, this test set contains 18 valence excitations, two Rydberg excitations, and two CT excitations. The valence excitations in this set refer to n → π^* and $\pi \rightarrow \pi^*$ excitations. The mean absolute errors (MAEs) and mean signed errors (MSEs) of excitation energies obtained from TDDFT, BSE/G_0W_0, BSE/$G_{RS}W_0$, BSE/$G_{RS}W_{RS}$, and BSE/evGW with HF, BLYP, PBE, B3LYP, PBE0, and PBEh(0.75) are shown in Figure 1 and Table 1. The PBE-based hybrid functional PBEh(0.75) that has 75% HF exchange is shown as the optimal starting point for G_0W_0 to predict IPs in the GW100 set.[104] The signed error is defined as the difference between the calculated value and the reference value, that is, $E^{calc} - E^{reference}$. Because this test set mainly contains valence excitations, TDDFT with conventional DFAs provides good accuracy. However, TDDFT based on the DFA with a large percentage of the HF exchange has large errors and can suffer from triplet instability. As evident from Figure 1, BSE/G_0W_0 greatly underestimates the excitation energies and provides large MAEs, which were also reported previously.[31,59] This error can be attributed to the overscreening problem in G_0W_0, that is, the screened interaction W is calculated with an underestimated KS gap.[31] The underestimated fundamental gap in G_0W_0 leads to the underestimated optical gap in BSE/G_0W_0. In addition, BSE/G_0W_0 has a strong starting point dependence. The difference between MAEs of BSE/G_0W_0 with GGA and hybrid functionals is larger than 0.7 eV. BSE/G_0W_0, based on PBEh(0.75), that is the optimal starting point for valence QP energy provides a small MAE of 0.27 eV. However, the percentage of the HF exchange needs to be reoptimized for excitations of different characters and different species.[32] Recent work has shown that the optimally tuned range-separated hybrid DFAs can be a good starting point for BSE/G_0W_0.[105] The BSE/$G_{RS}W_0$ approach improves upon BSE/G_0W_0. Using $G_{RS}W_0$ instead of G_0W_0, the MAEs are reduced by around 0.6 eV with GGA functionals and by around 0.3 eV with hybrid functionals. However, there is still an undesired starting point dependence in BSE/$G_{RS}W_0$ because the screened interaction in $G_{RS}W_0$ is calculated at the chosen DFA level. The BSE/$G_{RS}W_{RS}$ approach significantly outperforms BSE/G_0W_0 and BSE/$G_{RS}W_0$. The MAEs from BSE/$G_{RS}W_{RS}$ with conventional DFAs are around 0.4 eV. They are similar to the MAEs from TDDFT with hybrid functionals and are slightly better than the ones from BSE/evGW. BSE/$G_{RS}W_{RS}$ with the optimal starting point PBEh(0.75) provides the smallest MAE of 0.29 eV. As shown in Section 3 in the Supporting Information, fundamental gaps obtained from RS orbital energies are always larger than those obtained from KS orbital energies. By inserting the RS Green's function into the RPA equation to formulate the screened interaction, BSE/$G_{RS}W_{RS}$ greatly reduces the overscreening error and provides excellent accuracy. The starting point dependence in BSE/$G_{RS}W_{RS}$ is largely reduced, which is similar to BSE/evGW. The different DFAs induce only small changes of less than 0.1 eV in the BSE/$G_{RS}W_{RS}$ MAEs. We find that BSE/$G_{RS}W_{RS}$, BSE/G_0W_0, and BSE/evGW yield triplet excitation energies which are significantly too low, which is in agreement with previous work.[31]

Table 1. Total MAEs of Excitation Energies in the Truhlar−Gagliardi Test Set Obtained from TDDFT, BSE/G_0W_0, BSE/$G_{RS}W_0$, BSE/$G_{RS}W_{RS}$, and BSE/evGW Based on HF, BLYP, PBE, B3LYP, PBE0, and PBEh(0.75)[a]

	HF	BLYP	PBE	B3LYP	PBE0	PBEh
BSE/G_0W_0	0.76	1.43	1.40	0.99	0.88	0.27
BSE/$G_{RS}W_0$	0.76	0.83	0.82	0.67	0.61	0.28
BSE/$G_{RS}W_{RS}$	0.76	0.37	0.36	0.35	0.34	0.29
BSE/evGW	0.74	0.48	0.47	0.52	0.53	0.26
TDDFT	1.54	0.52	0.51	0.33	0.31	0.85

[a]Reference values for pNA and DMABN were taken from ref 94 and for the remaining molecules from ref 95. The reference values are the theoretical best estimates. The aug-cc-pVDZ basis set was used for naphthalene, pNA, and DMABN, and the aug-cc-pVTZ basis set was used for the remaining systems. B-TCNE was excluded due to the high computational cost. Total MAEs were calculated by averaging all systems with equal weights. The error for system i is defined as $\text{Error}_i = E_i^{calc} - E_i^{reference}$.

4.2. Stein CT Test Set. We further study the performance of BSE/$G_{RS}W_{RS}$ in predicting CT excitation energies by testing the Stein CT test set. This test set contains 12 intramolecular CT systems. The MAEs and MSEs of excitation energies obtained from TDDFT, BSE/G_0W_0, BSE/$G_{RS}W_0$, and BSE/$G_{RS}W_{RS}$ with HF, BLYP, PBE B3LYP, PBE0, and PBEh(0.75) are listed in Table 2. It shows that TDDFT with conventional DFAs fails to predict CT excitation energies due to the incorrect description of the long-range behavior. TDDFT with

Table 2. MAEs and MSEs of CT Excitation Energies in the Stein CT Test Set Obtained from TDDFT, BSE/G_0W_0, BSE/$G_{RS}W_0$, and BSE/$G_{RS}W_{RS}$ with HF, BLYP, PBE, B3LYP, PBE0, and PBEh(0.75)[a]

	HF		BLYP		PBE		B3LYP		PBE0		PBEh	
	MAE	MSE	MAE	MSE	MAE	MSE	MAE	MSE	MAE	MSE	MAE	MSE
TDDFT	0.78	0.78	1.44	−1.44	1.45	−1.45	1.16	−1.16	1.08	−1.08	0.19	0.02
BSE/G_0W_0	0.10	−0.06	1.28	−1.28	1.31	−1.31	0.74	−0.74	0.65	−0.65	0.14	0.09
BSE/$G_{RS}W_0$	0.10	−0.06	0.35	−0.35	0.35	−0.37	0.29	−0.28	0.29	−0.29	0.16	−0.15
BSE/$G_{RS}W_{RS}$	0.10	−0.06	0.17	0.14	0.18	0.11	0.14	0.09	0.17	0.14	0.11	−0.07

[a]All values in eV. Geometries were taken from ref 91. Experiment values in the gas phase were taken as the reference values.[91] Gas-phase experimental references were used. The error for system i is defined as $\text{Error}_i = E_i^{calc} - E_i^{experiment}$ The cc-pVDZ basis set was used.

https://doi.org/10.1021/acs.jctc.2c00686
J. Chem. Theory Comput. 2022, 18, 6637−6645

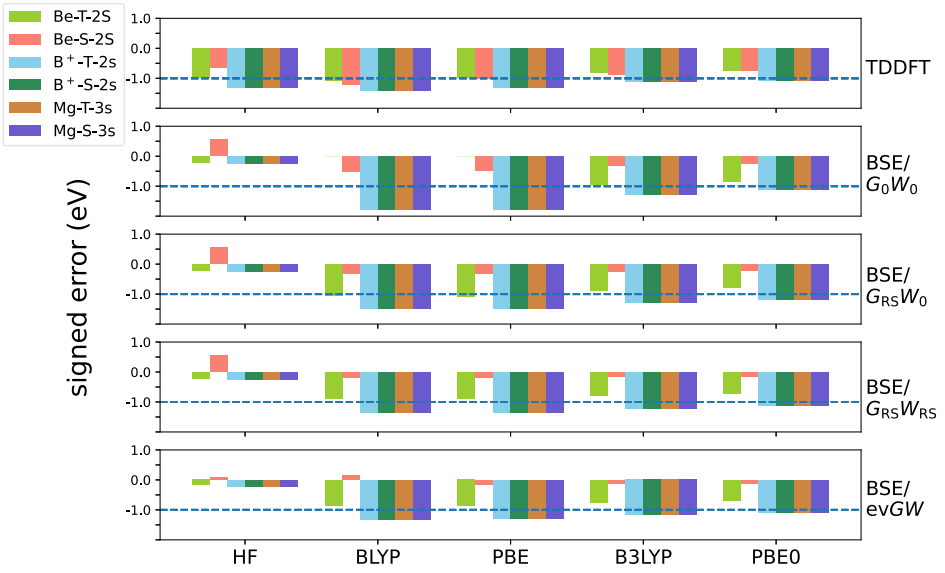

Figure 2. Signed errors of B^+, Be and Mg obtained from TDDFT, BSE/G_0W_0, BSE/$G_{RS}W_0$, BSE/$G_{RS}W_{RS}$, and BSE/evGW with HF, BLYP, PBE, B3LYP, and PBE0. All values in eV. Experimental values were taken as the reference values.[97] The aug-cc-pVQZ basis set was used. The signed error for system i is defined as $\text{Error}_i = E_i^{\text{calc}} - E_i^{\text{experiment}}$.

both GGA and hybrid functionals greatly underestimates the CT excitation energies and gives MAEs larger than 1.0 eV. TDDFT with PBEh(0.75) that has a large percentage of the HF exchange provides a small MAE of 0.19 eV. In addition, TDDFT has a strong starting point dependence. BSE/G_0W_0 provides improved results over TDDFT because of the correct long-range behavior from the screened interaction. However, BSE/G_0W_0 still suffers from a strong dependence on the choice of the DFA and yields relatively large errors. As shown in Section 6 in the Supporting Information, BSE/G_0W_0 always underestimates the excitation energies of CT systems. Slightly larger excitation energies can be obtained when using the TDA.[59] The BSE/$G_{RS}W_0$ approach improves again upon BSE/G_0W_0. Compared with BSE/G_0W_0, the MAEs of BSE/$G_{RS}W_0$ are 1.0 and 0.4 eV smaller with GGA and hybrid functionals, respectively. The dependence on the DFA is reduced to only 0.09 eV in the BSE/$G_{RS}W_0$ scheme. The BSE/$G_{RS}W_{RS}$ approach provides the most accurate results with the smallest starting point dependence. The MAEs of BSE/$G_{RS}W_{RS}$ with all tested DFAs are only around 0.15 eV, which are comparable to the accuracy of BSE/evGW as reported in ref 41. In addition, the dependence on the choice of the DFA in BSE/$G_{RS}W_{RS}$ is largely eliminated. The difference originating from using different DFAs is only around 0.04 eV.

4.3. Rydberg Excitations. We further investigate the performance of the BSE/$G_{RS}W_0$ and the BSE/$G_{RS}W_{RS}$ approaches for predicting Rydberg excitation energies of atomic systems by testing B^+, Be, and Mg. The signed errors of Rydberg excitation energies obtained from TDDFT, BSE/G_0W_0, BSE/$G_{RS}W_0$, BSE/$G_{RS}W_{RS}$, and BSE/evGW with HF, BLYP, PBE, B3LYP, and PBE0 are listed in Figure 2. Numerical results are shown in Section 7 in the Supporting Information. Similar to the CT excitation energies, it is well-known that TDDFT with common DFAs has relatively large errors for predicting Rydberg excitation energies.[31] The latter largely underestimates with GGA as well as hybrid functionals in TDDFT. Compared to TDDFT, the BSE/G_0W_0 approach yields only slightly better predictions, reducing the MAE by around 0.1 eV. TDDFT and BSE/G_0W_0 both show strong starting point dependence. BSE/$G_{RS}W_0$ slightly improves upon BSE/G_0W_0, reducing the MAE by 0.1 eV with respect to BSE/G_0W_0. The BSE/$G_{RS}W_{RS}$ approach provides further improvements over BSE/$G_{RS}W_0$. As shown in Section 7 in the Supporting Information and Figure 2, BSE/$G_{RS}W_{RS}$ shows significant improvements over TDDFT for predicting singlet Rydberg excitation energies with reduced errors around 0.4 eV. However, the improvements on triplet Rydberg excitation energies are small. The MAEs of BSE/$G_{RS}W_{RS}$ with all different DFAs are around 0.6 eV, which is close to the BSE/evGW level. The DFA starting point dependence is reduced to round 0.2 and 0.1 eV with BSE/$G_{RS}W_0$ and BSE/$G_{RS}W_{RS}$, respectively.

5. CONCLUSIONS

In this work, we applied the BSE formalism on top of the $G_{RS}W_{RS}$ method to calculate valence, Rydberg, and CT excitation energies of molecular systems. The $G_{RS}W_{RS}$ method provides improved fundamental gaps compared to G_0W_0 and largely reduces the dependence on the choice of the density functional approximation. In the BSE/$G_{RS}W_{RS}$ approach, the QP energies from $G_{RS}W_{RS}$ are used in BSE. For the Truhlar–Gagliardi test set, we found that BSE/$G_{RS}W_{RS}$ provides excellent accuracy for excitations of different characters (valence, CT, and Rydberg excitations) with MAEs around 0.4 eV. The accuracy of BSE/$G_{RS}W_{RS}$ is similar to TDDFT and slightly better than BSE/evGW. Using the Stein CT test set, we further showed that BSE/$G_{RS}W_{RS}$ is significantly more accurate for predicting CT excitation energies than BSE/G_0W_0 and TDDFT. We also found that the predictions compare well to BSE/evGW results reported in the literature.[41] We also showed that BSE/$G_{RS}W_{RS}$ predict accurate Rydberg excitation energies for atomic systems. We found for all three test sets that the dependence on the choice of the DFA is also largely eliminated. The computational cost of BSE/$G_{RS}W_{RS}$ is similar to BSE/G_0W_0, which has a much lower computational cost than BSE/evGW.

This work demonstrates that the BSE/$G_{RS}W_{RS}$ approach is accurate and efficient for predicting all three types of excitation

https://doi.org/10.1021/acs.jctc.2c00686
J. Chem. Theory Comput. 2022, 18, 6637−6645

energies of a broad range of systems. Therefore, the BSE/$G_{RS}W_{RS}$ approach is expected to expand the applicability of the BSE/*GW* approach.

■ ASSOCIATED CONTENT

Supporting Information

The Supporting Information is available free of charge at https://pubs.acs.org/doi/10.1021/acs.jctc.2c00686.

Fundamental gaps obtained from different *GW* method, errors of using the linearized QP equation in BSE, fundamental gaps obtained from KS-DFT and KS-DFT with RS, comparison of excitation energies obtained from BSE/$G_{RS}W_{RS}$ with and without the TDA, results of the Truhlar−Gagliardi test set, results of the Stein CT test set, and results of Rydberg excitation energies (PDF)

■ AUTHOR INFORMATION

Corresponding Author

Weitao Yang − *Department of Chemistry, Duke University, Durham, North Carolina 27708, United States;* orcid.org/0000-0001-5576-2828; Email: weitao.yang@duke.edu

Authors

Jiachen Li − *Department of Chemistry, Duke University, Durham, North Carolina 27708, United States;* orcid.org/0000-0002-9863-1091

Dorothea Golze − *Faculty of Chemistry and Food Chemistry, Technische Universität Dresden, 01062 Dresden, Germany;* orcid.org/0000-0002-2196-9350

Complete contact information is available at: https://pubs.acs.org/10.1021/acs.jctc.2c00686

Notes

The authors declare no competing financial interest.

■ ACKNOWLEDGMENTS

J.L. acknowledges the support from the National Institute of General Medical Sciences of the National Institutes of Health under award number R01-GM061870. D.G. acknowledges the Emmy Noether Programme of the German Research Foundation under project number 453275048. W.Y. acknowledges the support from the National Science Foundation (grant no. CHE-1900338).

■ REFERENCES

(1) Velema, W. A.; van der Berg, J. P.; Hansen, M. J.; Szymanski, W.; Driessen, A. J. M.; Feringa, B. L. Optical Control of Antibacterial Activity. *Nat. Chem.* **2013**, *5*, 924−928.

(2) Beharry, A. A.; Sadovski, O.; Woolley, G. A. Azobenzene Photoswitching without Ultraviolet Light. *J. Am. Chem. Soc.* **2011**, *133*, 19684−19687.

(3) Shalabi, A. S.; El Mahdy, A. M.; Taha, H. O.; Soliman, K. A. The Effects of Macrocycle and Anchoring Group Replacements on the Performance of Porphyrin Based Sensitizer: DFT and TD-DFT Study. *J. Phys. Chem. Solids* **2015**, *76*, 22−33.

(4) Zhang, C.-R.; Liu, Z.-J.; Chen, Y.-H.; Chen, H.-S.; Wu, Y.-Z.; Feng, W.; Wang, D.-B. DFT and TD-DFT Study on Structure and Properties of Organic Dye Sensitizer TA-St-CA. *Curr. Appl. Phys.* **2010**, *10*, 77−83.

(5) Runge, E.; Gross, E. K. U. Density-Functional Theory for Time-Dependent Systems. *Phys. Rev. Lett.* **1984**, *52*, 997−1000.

(6) Casida, M. E.Time-Dependent Density Functional Response Theory for Molecules. *Recent Advances in Computational Chemistry*; World Scientific, 1995; Vol. *1*; pp 155−192.

(7) Ullrich, C. A.*Time-Dependent Density-Functional Theory: Concepts and Applications*; OUP Oxford, 2011.

(8) Casida, M. E. Time-Dependent Density-Functional Theory for Molecules and Molecular Solids. *J. Mol. Struct.: THEOCHEM* **2009**, *914*, 3−18.

(9) Casida, M.; Ipatov, A.; Cordova, F.Linear-Response Time-Dependent Density Functional Theory for Open-Shell Molecules. *Time-Dependent Density Functional Theory*; Marques, M. A., Ullrich, C. A., Nogueira, F., Rubio, A., Burke, K., Gross, E. K. U., Eds.; Lecture Notes in Physics; Springer: Berlin, Heidelberg, 2006; pp 243−257.

(10) Laurent, A. D.; Jacquemin, D. TD-DFT Benchmarks: A Review. *Int. J. Quantum Chem.* **2013**, *113*, 2019−2039.

(11) Tozer, D. J. Relationship between long-range charge-transfer excitation energy error and integer discontinuity in Kohn-Sham theory. *J. Chem. Phys.* **2003**, *119*, 12697−12699.

(12) Dreuw, A.; Weisman, J. L.; Head-Gordon, M. Long-Range Charge-Transfer Excited States in Time-Dependent Density Functional Theory Require Non-Local Exchange. *J. Chem. Phys.* **2003**, *119*, 2943−2946.

(13) Leininger, T.; Stoll, H.; Werner, H.-J.; Savin, A. Combining Long-Range Configuration Interaction with Short-Range Density Functionals. *Chem. Phys. Lett.* **1997**, *275*, 151−160.

(14) Besley, N. A.; Peach, M. J. G.; Tozer, D. J. Time-Dependent Density Functional Theory Calculations of near-Edge X-ray Absorption Fine Structure with Short-Range Corrected Functionals. *Phys. Chem. Chem. Phys.* **2009**, *11*, 10350−10358.

(15) Peach, M. J. G.; Benfield, P.; Helgaker, T.; Tozer, D. J. Excitation Energies in Density Functional Theory: An Evaluation and a Diagnostic Test. *J. Chem. Phys.* **2008**, *128*, 044118.

(16) Ai, W.; Fang, W.-H.; Su, N. Q. The Role of Range-Separated Correlation in Long-Range Corrected Hybrid Functionals. *J. Phys. Chem. Lett.* **2021**, *12*, 1207−1213.

(17) Slater, J. C. Note on Hartree's Method. *Phys. Rev.* **1930**, *35*, 210−211.

(18) Szabo, A.; Ostlund, N. S.*Modern Quantum Chemistry: Introduction to Advanced Electronic Structure Theory*; Courier Corporation, 2012.

(19) Zhao, Y.; Truhlar, D. G. Density Functional for Spectroscopy: No Long-Range Self-Interaction Error, Good Performance for Rydberg and Charge-Transfer States, and Better Performance on Average than B3LYP for Ground States. *J. Phys. Chem. A* **2006**, *110*, 13126−13130.

(20) Leang, S. S.; Zahariev, F.; Gordon, M. S. Benchmarking the Performance of Time-Dependent Density Functional Methods. *J. Chem. Phys.* **2012**, *136*, 104101.

(21) Kaur, J.; Ospadov, E.; Staroverov, V. N. What Is the Accuracy Limit of Adiabatic Linear-Response TDDFT Using Exact Exchange-Correlation Potentials and Approximate Kernels? *J. Chem. Theory Comput.* **2019**, *15*, 4956−4964.

(22) Chen, Z.; Zhang, D.; Jin, Y.; Yang, Y.; Su, N. Q.; Yang, W. Multireference Density Functional Theory with Generalized Auxiliary Systems for Ground and Excited States. *J. Phys. Chem. Lett.* **2017**, *8*, 4479−4485.

(23) Li, J.; Chen, Z.; Yang, W. Multireference Density Functional Theory for Describing Ground and Excited States with Renormalized Singles. *J. Phys. Chem. Lett.* **2022**, *13*, 894−903.

(24) Hait, D.; Head-Gordon, M. Orbital Optimized Density Functional Theory for Electronic Excited States. *J. Phys. Chem. Lett.* **2021**, *12*, 4517−4529.

(25) Horbatenko, Y.; Sadiq, S.; Lee, S.; Filatov, M.; Choi, C. H. Mixed-Reference Spin-Flip Time-Dependent Density Functional Theory (MRSF-TDDFT) as a Simple yet Accurate Method for Diradicals and Diradicaloids. *J. Chem. Theory Comput.* **2021**, *17*, 848−859.

(26) Sham, L. J.; Rice, T. M. Many-Particle Derivation of the Effective-Mass Equation for the Wannier Exciton. *Phys. Rev.* **1966**, *144*, 708−714.
(27) Hanke, W.; Sham, L. J. Many-Particle Effects in the Optical Excitations of a Semiconductor. *Phys. Rev. Lett.* **1979**, *43*, 387−390.
(28) Salpeter, E. E.; Bethe, H. A. A Relativistic Equation for Bound-State Problems. *Phys. Rev.* **1951**, *84*, 1232−1242.
(29) Hedin, L. New Method for Calculating the One-Particle Green's Function with Application to the Electron-Gas Problem. *Phys. Rev.* **1965**, *139*, A796−A823.
(30) Martin, R. M.; Reining, L.; Ceperley, D. M.*Interacting Electrons*; Cambridge University Press, 2016.
(31) Blase, X.; Duchemin, I.; Jacquemin, D.; Loos, P.-F. The Bethe-Salpeter Equation Formalism: From Physics to Chemistry. *J. Phys. Chem. Lett.* **2020**, *11*, 7371−7382.
(32) Yao, Y.; Golze, D.; Rinke, P.; Blum, V.; Kanai, Y. All-Electron BSE@GW Method for K-Edge Core Electron Excitation Energies. *J. Chem. Theory Comput.* **2022**, *18*, 1569.
(33) Reining, L. The GW Approximation: Content, Successes and Limitations. *WIREs Comput. Mol. Sci* **2018**, *8*, No. e1344.
(34) Golze, D.; Dvorak, M.; Rinke, P. The GW Compendium: A Practical Guide to Theoretical Photoemission Spectroscopy. *Front. Chem.* **2019**, *7*, 377.
(35) Loos, P.-F.; Romaniello, P. Static and dynamic Bethe-Salpeter equations in the T-matrix approximation. *J. Chem. Phys.* **2022**, *156*, 164101.
(36) Jacquemin, D.; Duchemin, I.; Blondel, A.; Blase, X. Benchmark of Bethe-Salpeter for Triplet Excited-States. *J. Chem. Theory Comput.* **2017**, *13*, 767−783.
(37) Escudero, D.; Duchemin, I.; Blase, X.; Jacquemin, D. Modeling the Photochrome-TiO2 Interface with Bethe-Salpeter and Time-Dependent Density Functional Theory Methods. *J. Phys. Chem. Lett.* **2017**, *8*, 936−940.
(38) Jacquemin, D.; Duchemin, I.; Blase, X. Is the Bethe-Salpeter Formalism Accurate for Excitation Energies? Comparisons with TD-DFT, CASPT2, and EOM-CCSD. *J. Phys. Chem. Lett.* **2017**, *8*, 1524−1529.
(39) Azarias, C.; Duchemin, I.; Blase, X.; Jacquemin, D. Bethe-Salpeter Study of Cationic Dyes: Comparisons with ADC(2) and TD-DFT. *J. Chem. Phys.* **2017**, *146*, 034301.
(40) Azarias, C.; Habert, C.; Budzák, Š.; Blase, X.; Duchemin, I.; Jacquemin, D. Calculations of n→π^* Transition Energies: Comparisons Between TD-DFT, ADC, CC, CASPT2, and BSE/GW Descriptions. *J. Phys. Chem. A* **2017**, *121*, 6122−6134.
(41) Blase, X.; Attaccalite, C. Charge-Transfer Excitations in Molecular Donor-Acceptor Complexes within the Many-Body Bethe-Salpeter Approach. *Appl. Phys. Lett.* **2011**, *99*, 171909.
(42) Gatti, M.; Sottile, F.; Reining, L. Electron-Hole Interactions in Correlated Electron Materials: Optical Properties of Vanadium Dioxide from First Principles. *Phys. Rev. B: Condens. Matter Mater. Phys.* **2015**, *91*, 195137.
(43) Cudazzo, P.; Sponza, L.; Giorgetti, C.; Reining, L.; Sottile, F.; Gatti, M. Exciton Band Structure in Two-Dimensional Materials. *Phys. Rev. Lett.* **2016**, *116*, 066803.
(44) Sottile, F.; Marsili, M.; Olevano, V.; Reining, L. Efficientab initiocalculations of bound and continuum excitons in the absorption spectra of semiconductors and insulators. *Phys. Rev. B: Condens. Matter Mater. Phys.* **2007**, *76*, 161103.
(45) Jiang, X.; Zheng, Q.; Lan, Z.; Saidi, W. A.; Ren, X.; Zhao, J. Real-Time GW-BSE Investigations on Spin-Valley Exciton Dynamics in Monolayer Transition Metal Dichalcogenide. *Sci. Adv.* **2021**, *7*, No. eabf3759.
(46) Liu, C.; Kloppenburg, J.; Yao, Y.; Ren, X.; Appel, H.; Kanai, Y.; Blum, V. All-Electron Ab Initio Bethe-Salpeter Equation Approach to Neutral Excitations in Molecules with Numeric Atom-Centered Orbitals. *J. Chem. Phys.* **2020**, *152*, 044105.
(47) Dvorak, M.; Golze, D.; Rinke, P. Quantum Embedding Theory in the Screened Coulomb Interaction: Combining Configuration Interaction with GW/BSE. *Phys. Rev. Mater.* **2019**, *3*, 070801.
(48) Monino, E.; Loos, P.-F. Spin-Conserved and Spin-Flip Optical Excitations from the Bethe-Salpeter Equation Formalism. *J. Chem. Theory Comput.* **2021**, *17*, 2852−2867.
(49) Loos, P.-F.; Blase, X. Dynamical correction to the Bethe-Salpeter equation beyond the plasmon-pole approximation. *J. Chem. Phys.* **2020**, *153*, 114120.
(50) van Setten, M. J.; Weigend, F.; Evers, F. The GW-Method for Quantum Chemistry Applications: Theory and Implementation. *J. Chem. Theory Comput.* **2013**, *9*, 232−246.
(51) Golze, D.; Wilhelm, J.; van Setten, M. J.; Rinke, P. Core-Level Binding Energies from GW: An Efficient Full-Frequency Approach within a Localized Basis. *J. Chem. Theory Comput.* **2018**, *14*, 4856−4869.
(52) Ren, X.; Rinke, P.; Blum, V.; Wieferink, J.; Tkatchenko, A.; Sanfilippo, A.; Reuter, K.; Scheffler, M. Resolution-of-identity approach to Hartree-Fock, hybrid density functionals, RPA, MP2 andGWwith numeric atom-centered orbital basis functions. *New J. Phys.* **2012**, *14*, 053020.
(53) Duchemin, I.; Blase, X. Robust Analytic-Continuation Approach to Many-Body GW Calculations. *J. Chem. Theory Comput.* **2020**, *16*, 1742−1756.
(54) Wilhelm, J.; Golze, D.; Talirz, L.; Hutter, J.; Pignedoli, C. A. Toward GW Calculations on Thousands of Atoms. *J. Phys. Chem. Lett.* **2018**, *9*, 306−312.
(55) Förster, A.; Visscher, L. Low-Order Scaling G0W0 by Pair Atomic Density Fitting. *J. Chem. Theory Comput.* **2020**, *16*, 7381−7399.
(56) Wilhelm, J.; Seewald, P.; Golze, D. Low-Scaling GW with Benchmark Accuracy and Application to Phosphorene Nanosheets. *J. Chem. Theory Comput.* **2021**, *17*, 1662−1677.
(57) Duchemin, I.; Blase, X. Cubic-Scaling All-Electron GW Calculations with a Separable Density-Fitting Space-Time Approach. *J. Chem. Theory Comput.* **2021**, *17*, 2383−2393.
(58) Ziaei, V.; Bredow, T. GW-BSE Approach on S1 Vertical Transition Energy of Large Charge Transfer Compounds: A Performance Assessment. *J. Chem. Phys.* **2016**, *145*, 174305.
(59) Li, J.; Jin, Y.; Su, N. Q.; Yang, W. Combining localized orbital scaling correction and Bethe-Salpeter equation for accurate excitation energies. *J. Chem. Phys.* **2022**, *156*, 154101.
(60) Bruneval, F.; Hamed, S. M.; Neaton, J. B. A Systematic Benchmark of the Ab Initio Bethe-Salpeter Equation Approach for Low-Lying Optical Excitations of Small Organic Molecules. *J. Chem. Phys.* **2015**, *142*, 244101.
(61) van Schilfgaarde, M.; Kotani, T.; Faleev, S. Quasiparticle Self-Consistent GW Theory. *Phys. Rev. Lett.* **2006**, *96*, 226402.
(62) Kaplan, F.; Harding, M. E.; Seiler, C.; Weigend, F.; Evers, F.; van Setten, M. J. Quasi-Particle Self-Consistent GW for Molecules. *J. Chem. Theory Comput.* **2016**, *12*, 2528−2541.
(63) Caruso, F.; Rinke, P.; Ren, X.; Scheffler, M.; Rubio, A. Unified Description of Ground and Excited States of Finite Systems: The Self-Consistent GW Approach. *Phys. Rev. B: Condens. Matter Mater. Phys.* **2012**, *86*, 081102.
(64) Caruso, F.; Rinke, P.; Ren, X.; Rubio, A.; Scheffler, M. Self-Consistent GW: All-electron Implementation with Localized Basis Functions. *Phys. Rev. B: Condens. Matter Mater. Phys.* **2013**, *88*, 075105.
(65) Jacquemin, D.; Duchemin, I.; Blase, X. Assessment of the Convergence of Partially Self-Consistent BSE/GW Calculations. *Mol. Phys.* **2016**, *114*, 957−967.
(66) Véril, M.; Romaniello, P.; Berger, J. A.; Loos, P.-F. Unphysical Discontinuities in GW Methods. *J. Chem. Theory Comput.* **2018**, *14*, 5220−5228.
(67) Monino, E.; Loos, P.-F. Unphysical Discontinuities, Intruder States and Regularization in GW Methods. *J. Chem. Phys.* **2022**, *156*, 231101.
(68) Li, C.; Zheng, X.; Su, N. Q.; Yang, W. Localized Orbital Scaling Correction for Systematic Elimination of Delocalization Error in Density Functional Approximations. *Natl. Sci. Rev.* **2018**, *5*, 203−215.

https://doi.org/10.1021/acs.jctc.2c00686
J. Chem. Theory Comput. 2022, 18, 6637−6645

(69) Elliott, J. D.; Colonna, N.; Marsili, M.; Marzari, N.; Umari, P. Koopmans Meets Bethe-Salpeter: Excitonic Optical Spectra without GW. *J. Chem. Theory Comput.* **2019**, *15*, 3710−3720.
(70) Jin, Y.; Su, N. Q.; Yang, W. Renormalized Singles Green's Function for Quasi-Particle Calculations beyond the G0W0 Approximation. *J. Phys. Chem. Lett.* **2019**, *10*, 447−452.
(71) Li, J.; Jin, Y.; Rinke, P.; Yang, W.; Golze, D.Benchmark of GW Methods for Core-Level Binding Energies. **2022**, arXiv preprint arXiv:2206.05627
(72) Hohenberg, P.; Kohn, W. Inhomogeneous Electron Gas. *Phys. Rev.* **1964**, *136*, B864−B871.
(73) Kohn, W.; Sham, L. J. Self-Consistent Equations Including Exchange and Correlation Effects. *Phys. Rev.* **1965**, *140*, A1133−A1138.
(74) Parr, R. G.; Weitao, Y.*Density-Functional Theory of Atoms and Molecules*; Oxford University Press, 1989.
(75) Bruneval, F.; Marques, M. A. L. Benchmarking the Starting Points of the GW Approximation for Molecules. *J. Chem. Theory Comput.* **2013**, *9*, 324−329.
(76) Li, J.; Chen, Z.; Yang, W. Renormalized Singles Green's Function in the T-Matrix Approximation for Accurate Quasiparticle Energy Calculation. *J. Phys. Chem. Lett.* **2021**, *12*, 6203−6210.
(77) Ren, X.; Tkatchenko, A.; Rinke, P.; Scheffler, M. Beyond the Random-Phase Approximation for the Electron Correlation Energy: The Importance of Single Excitations. *Phys. Rev. Lett.* **2011**, *106*, 153003.
(78) Ren, X.; Rinke, P.; Scuseria, G. E.; Scheffler, M. Renormalized Second-Order Perturbation Theory for the Electron Correlation Energy: Concept, Implementation, and Benchmarks. *Phys. Rev. B: Condens. Matter Mater. Phys.* **2013**, *88*, 035120.
(79) Paier, J.; Ren, X.; Rinke, P.; Scuseria, G. E.; Grüneis, A.; Kresse, G.; Scheffler, M. Assessment of Correlation Energies Based on the Random-Phase Approximation. *New J. Phys.* **2012**, *14*, 043002.
(80) Li, J.; Yang, W.Renormalized Singles with Correlation in GW Green's Function Theory for Accurate Quasiparticle Energies. **2022**, arXiv preprint arXiv:2207.06520
(81) Loos, P.-F.; Romaniello, P.; Berger, J. A. Green Functions and Self-Consistency: Insights From the Spherium Model. *J. Chem. Theory Comput.* **2018**, *14*, 3071−3082.
(82) Krause, K.; Klopper, W. Implementation of the Bethe−Salpeter equation in the TURBOMOLE program. *J. Comput. Chem.* **2017**, *38*, 383−388.
(83) Ghosh, S. K.; Chattaraj, P. K.*Concepts and Methods in Modern Theoretical Chemistry: Electronic Structure and Reactivity*; CRC Press, 2016.
(84) Stratmann, R. E.; Scuseria, G. E.; Frisch, M. J. An Efficient Implementation of Time-Dependent Density-Functional Theory for the Calculation of Excitation Energies of Large Molecules. *J. Chem. Phys.* **1998**, *109*, 8218−8224.
(85) Davidson, E. R. The Iterative Calculation of a Few of the Lowest Eigenvalues and Corresponding Eigenvectors of Large Real-Symmetric Matrices. *J. Comput. Phys.* **1975**, *17*, 87−94.
(86) See http://www.qm4d.info, for an in-house program for QM/MM simulations (accessed June 30, 2022).
(87) Faber, C.; Boulanger, P.; Duchemin, I.; Attaccalite, C.; Blase, X. Many-body Green's function GW and Bethe-Salpeter study of the optical excitations in a paradigmatic model dipeptide. *J. Chem. Phys.* **2013**, *139*, 194308.
(88) Rocca, D.; Lu, D.; Galli, G. Ab initio calculations of optical absorption spectra: Solution of the Bethe-Salpeter equation within density matrix perturbation theory. *J. Chem. Phys.* **2010**, *133*, 164109.
(89) Duchemin, I.; Deutsch, T.; Blase, X. Short-Range to Long-Range Charge-Transfer Excitations in the Zincbacteriochlorin-Bacteriochlorin Complex: A Bethe-Salpeter Study. *Phys. Rev. Lett.* **2012**, *109*, 167801.
(90) Hoyer, C. E.; Ghosh, S.; Truhlar, D. G.; Gagliardi, L. Multiconfiguration Pair-Density Functional Theory Is as Accurate as CASPT2 for Electronic Excitation. *J. Phys. Chem. Lett.* **2016**, *7*, 586−591.
(91) Stein, T.; Kronik, L.; Baer, R. Reliable Prediction of Charge Transfer Excitations in Molecular Complexes Using Time-Dependent Density Functional Theory. *J. Am. Chem. Soc.* **2009**, *131*, 2818−2820.
(92) Dunning, T. H. Gaussian Basis Sets for Use in Correlated Molecular Calculations. I. The Atoms Boron through Neon and Hydrogen. *J. Chem. Phys.* **1989**, *90*, 1007−1023.
(93) Kendall, R. A.; Dunning, T. H.; Harrison, R. Electron affinities of the first-row atoms revisited. Systematic basis sets and wave functions. *J. Chem. Phys.* **1992**, *96*, 6796−6806.
(94) Gui, X.; Holzer, C.; Klopper, W. Accuracy Assessment of GW Starting Points for Calculating Molecular Excitation Energies Using the Bethe-Salpeter Formalism. *J. Chem. Theory Comput.* **2018**, *14*, 2127−2136.
(95) Véril, M.; Scemama, A.; Caffarel, M.; Lipparini, F.; Boggio-Pasqua, M.; Jacquemin, D.; Loos, P.-F. QUESTDB: A Database of Highly Accurate Excitation Energies for the Electronic Structure Community. *Wiley Interdiscip. Rev.: Comput. Mol. Sci.* **2021**, *11*, No. e1517.
(96) Loos, P.-F.; Comin, M.; Blase, X.; Jacquemin, D. Reference Energies for Intramolecular Charge-Transfer Excitations. *J. Chem. Theory Comput.* **2021**, *17*, 3666−3686.
(97) Xu, X.; Yang, K. R.; Truhlar, D. G. Testing Noncollinear Spin-Flip, Collinear Spin-Flip, and Conventional Time-Dependent Density Functional Theory for Predicting Electronic Excitation Energies of Closed-Shell Atoms. *J. Chem. Theory Comput.* **2014**, *10*, 2070−2084.
(98) Frisch, M. J.; et al.*Gaussian16*, Revision A.03; Gaussian Inc: Wallingford CT. 2016.
(99) Weigend, F. Accurate Coulomb-fitting Basis Sets for H to Rn. *Phys. Chem. Chem. Phys.* **2006**, *8*, 1057.
(100) Eichkorn, K.; Treutler, O.; Öhm, H.; Häser, M.; Ahlrichs, R. Auxiliary Basis Sets to Approximate Coulomb Potentials. *Chem. Phys. Lett.* **1995**, *240*, 283−290.
(101) Feller, D. The Role of Databases in Support of Computational Chemistry Calculations. *J. Comput. Chem.* **1996**, *17*, 1571−1586.
(102) Schuchardt, K. L.; Didier, B. T.; Elsethagen, T.; Sun, L.; Gurumoorthi, V.; Chase, J.; Li, J.; Windus, T. L. Basis Set Exchange: A Community Database for Computational Sciences. *J. Chem. Inf. Model.* **2007**, *47*, 1045−1052.
(103) Pritchard, B. P.; Altarawy, D.; Didier, B.; Gibson, T. D.; Windus, T. L. New Basis Set Exchange: An Open, Up-to-Date Resource for the Molecular Sciences Community. *J. Chem. Inf. Model.* **2019**, *59*, 4814−4820.
(104) Bruneval, F.; Dattani, N.; van Setten, M. J. The GW Miracle in Many-Body Perturbation Theory for the Ionization Potential of Molecules. *Front. Chem.* **2021**, *9*, 749779.
(105) McKeon, C. A.; Hamed, S. M.; Bruneval, F.; Neaton, J. B. An Optimally Tuned Range-Separated Hybrid Starting Point for Ab Initio GW plus Bethe−Salpeter Equation Calculations of Molecules. *J. Chem. Phys.* **2022**, *157*, 074103.

https://doi.org/10.1021/acs.jctc.2c00686
J. Chem. Theory Comput. 2022, 18, 6637−6645